Electronic Supplementary Material (ESI) for Nanoscale.
This journal is © The Royal Society of Chemistry 2021

Quantifying thermal transport in buried semiconductor nanostructures via Cross-Sectional Scanning Thermal Microscopy

Jean Spièce,[†] Charalambos Evangeli,[†] Alex J. Robson,[†] Alexandros El Sachat,[‡,▽] Linda Haenel,[§] M. Isabel Alonso,[°] Miquel Garriga,[°] Benjamin J. Robinson,[†] Michael Oehme,[§] Jörg Schulz,[§] Francesc Alzina,[‡] Clivia Sotomayor Torres,[‡] Oleg V. Kolosov[,†]*

[†]Physics Department, Lancaster University, LA1 4YB, Lancaster, UK, [‡]Catalan Institute of Nanoscience and Nanotechnology (ICN2), CSIC and Barcelona Institute of Science and Technology, Campus UAB, 08193 Barcelona, Spain, [▽]Dept. of Physics, Universitat Autònoma de Barcelona, Campus UAB, 08193 Bellaterra, Spain, [°]Institut de Ciència de Materials de Barcelona (ICMAB-CSIC), Campus de la UAB, 08193 Bellaterra, Spain, [§]Institute of Semiconductor Engineering, University of Stuttgart, Pfaffenwaldring 47, 70569 Stuttgart, Germany.

[*]To whow correspondence should be addressed; Email: o.kolosov@lancaster.ac.uk

(Supporting Note 1) Spreading resistance fitting method

Eq 1 in the main text as a major unknown, typical for any SThM conductance measurement: the effective interface resistance between the probe and the sample, R_c. The second terms, R_s depends on the sample structure and materials and is often the target of the experiment. In our case, the spreading resistance is a function of the thickness $R_s = R_s(t)$ and we assume that R_c remains constant for the same material. To remove the contribution of R_c in the experimental data, we can define a new fitting function accounting only for the spreading resistance effect:

$$f(t) = R_X - R_{X0} = R_c + R_s(t) - (R_c + R_s(t_0)) = R_s(t) - R_s(t_0)$$

where t_0 is a given reference thickness. Using *f(t)* to fit the data removes temporarily R_c as all variations in the data come from the spreading resistance variations only. R_c can be obtained afterwards by simply finding the offset to match the measured resistance.

(Supporting Note 2) Quantifying thermal conductance anisotropy

We use Finite Element Analysis, FEA, method to quantify thermal conductance anisotropy of gradient Si_xGe_{1-x}. This material is a good candidate for high temperature thermoelectrics where the independent increase of the Seebeck coefficient and reduction of thermal conductivity can be achieved. The layer Si_xGe_{1-x} was grown by molecular beam epitaxy (MBE) on a Si substrate with a Ge concentration increasing from 0% at the bottom to 23% at the top surface, $220\ nm$ away from the substrate.

For FEA, the gradient nano-cross-sectioning processed wedge-shaped layer was modeled by a large number of uniform layers with gradually increasing Ge concentration to decrease the computation time (see next section). In this model, we assumed a growth parameters derived linear

increase of Ge content (x_{Ge}) with the height inside the layer (t) resulting on $x_{Ge} = t * \frac{0.23}{220}$ as a function of thickness t. A well-established expression for the alloy thermal conductivity was taken from the literature[34-36] and implemented in our FEA simulation.

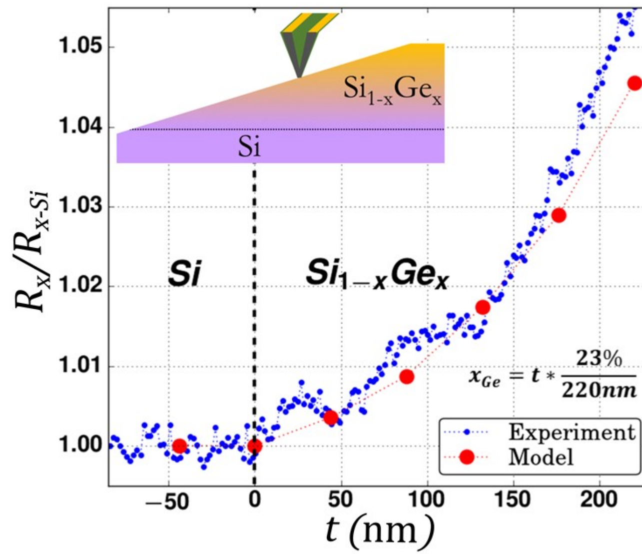

Figure S1. Thermal resistance of the nano-cross-sectioned $Si_{1-x}Ge_x$ on Si sample. The modelled and measured thermal resistances R_x are normalized to one of Si substrate, R_{x-Si}, and presented as a function of position in the layer and, correspondingly, increasing Ge composition. The contact radius was deduced from the contact to Si, and no other fitting parameters were used.

In Figure S1, experimental results of the total thermal resistance in the $SiGe_x$ gradient layer normalized to thermal resistance Si are compared to the modelling. In the model, the contact thermal resistance R_c is assumed constant and no other fitting parameters were used. Thermal

properties of bulk $Si_{1-x}Ge_x$ alloys have been studied extensively. Its thermal conductivity changes with initial increase of Ge concentration[27] with a significant reduction compared to the bulk values of either Si and Ge. When the SThM probe scans across the different layers, the thermal resistance at the tip apex is affected by the thermal transport in a particular nanoscale volume in the 3D space of the sample. As can be seen, the model and the experiment provide a very remarkable correlation, given the absence of the fitting parameters. When moving towards the higher Ge content, a slight deviation is observed that may be linked with the increase of the contact thermal resistance, or reduced thermal conductivity in thin films[27, 31].

We exclude the possibility of ballistic thermal transport since the phonon mean free path Λ in the system is greatly reduced compared to bulk values due to interface scattering and impurities[27]. Diffusive transport assumption remains valid if the heat source dimension a is bigger than the Λ, meaning that the system Knudsen number ($Kn=\Lambda/a$) is smaller than 1 ($Kn<<1$). Except for dislocation free Si where Λ~300 nm[37], MFPs are usually smaller than 50 nm, the typical effective contact radius[29].

(Supporting Note 3) Finite element modelling of anisotropic structure

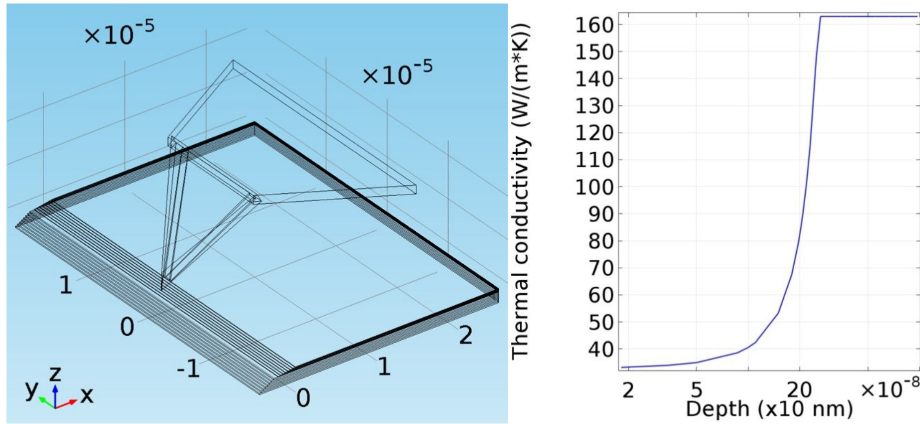

Figure S2: left: Finite Element model geometry with several steps mimicking the cross-sectioned surface.; Right: thermal conductivity profile across the model steps.

Fig. S1 shows the thermal conductivity inside the material from top to bottom set as material property for the first 220 nm. On the top of the layer, the thermal conductivity is that of $Si_{0.97}Ge_{0.23}$ and as we go deeper inside the steps, it is increasing toward the bulk Si thermal conductivity value.

Using the same thermal conductivity profile across the materials, we can model the spreading resistance of a heat source on the surface. The spreading resistance is defined as

$$R_{spr} = \frac{T_{av} - T_0}{Q}$$

where T_{av} is the average temperature over the heat source surface and T_0 is the boundary temperature. Q is the total power set on the heat source. We can then model the spreading resistance as a function of height probed. Due to the thermal conductivity profile, the material under the heat source has a gradually increasing thermal conductivity. It can be seen on Fig. S2

that the spreading resistance is first increasing and then reducing with increasing height (blue triangles). Whereas with a constant conductivity, the resistance increases (red circles).

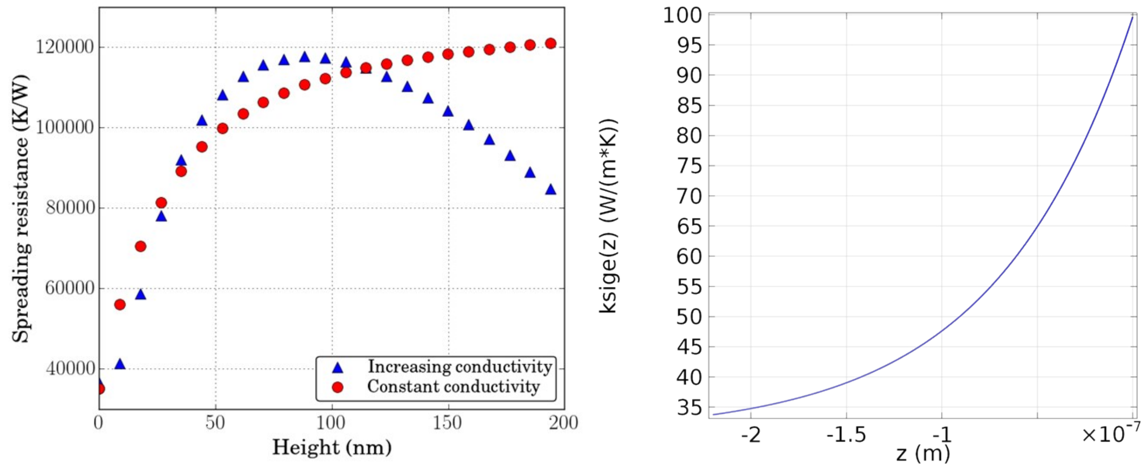

Figure S3: Thermal spreading resistance computed for a constant and an increasing layer thermal conductivity and the increasing layer thermal conductivity distribution.

(Supporting Note 4) Data and measurements results on thin films on substrate

Figure S4 presents the SThM maps and thermal resistance profiles of the 60 nm spin-on carbon and 10 nm spin-on glass samples. Using the fitting method presented, we could obtain the thermal properties of these samples.

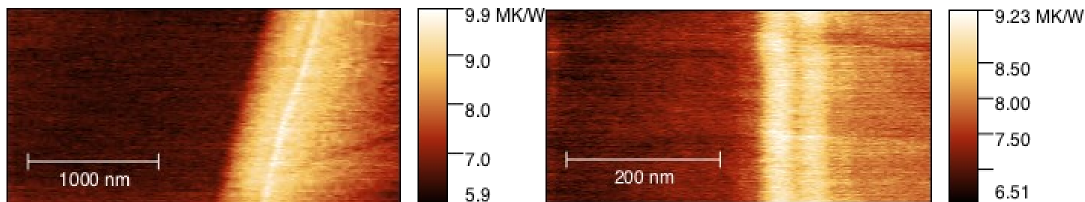

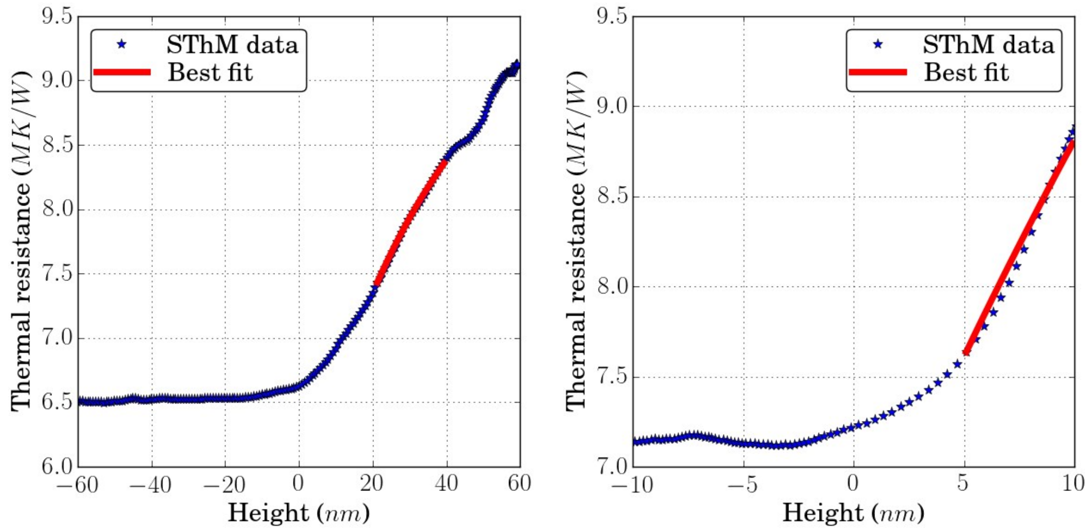

Figure S4: Thermal maps and resistance profiles for the 60 nm spin-on carbon and 10 nm spin-on glass samples. The fitted data is shown in red.

(Supporting Note 5) Air-vacuum measurement comparison

To confirm the accuracy of the measurements performed in air, we compared experiments performed in both environment on the same sample (see Fig. S4). Similar results were obtained and features observed on the surface. We note a slightly better sensitivity in vacuum which can be attributed to a smaller effective contact area, as expected in vacuum. However, the good agreement between both measurements supports the measurements performed in air as the air thermal resistance variations don't affect the profile measured.

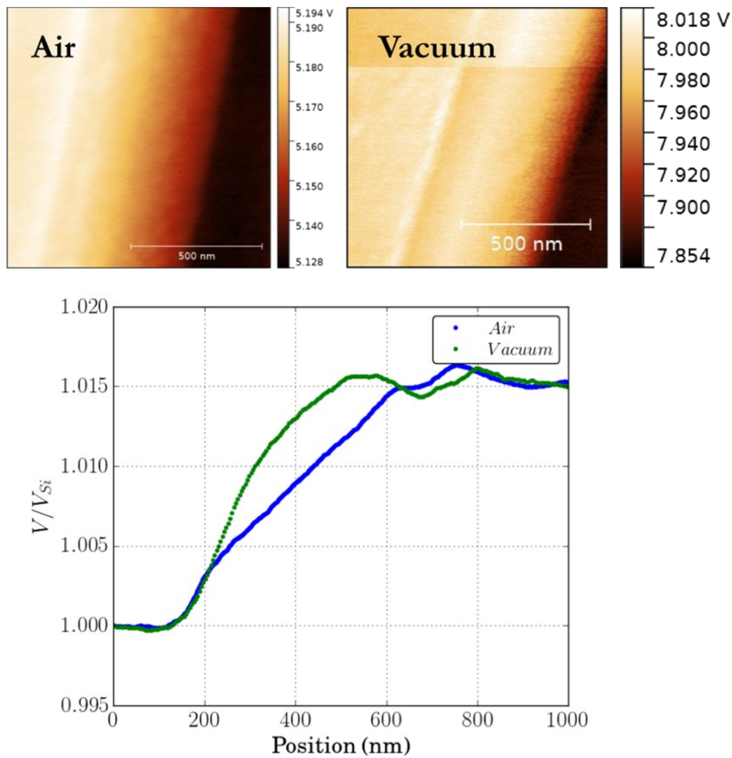

Figure S5: Comparison of air and vacuum measurements. Top: thermal maps of the same sample in air and vacuum. Bottom: SThM profiles normalized to the substrate and top surface measurement.

(Supporting Note 6) Ge concentration measurement

The Ge content was measurement with Secondary ion mass spectroscopy (SIMS) in the multilayer sample of $Si/Si_xGe_{1-x}/Ge/Ge_ySn_{1-y}$. Results are shown in figure S6. It can be observed that from about 325 nm, the Ge concentration is 0%. This corresponds to the silicon substrate. Then between 325 nm and 250 nm the Ge content increases and saturates to about 90% with a remaining 10% of Si content that reflects the Si diffusion during the Ge growth process. From 250 nm, the Ge virtual substrate starts and contains 100% Ge.

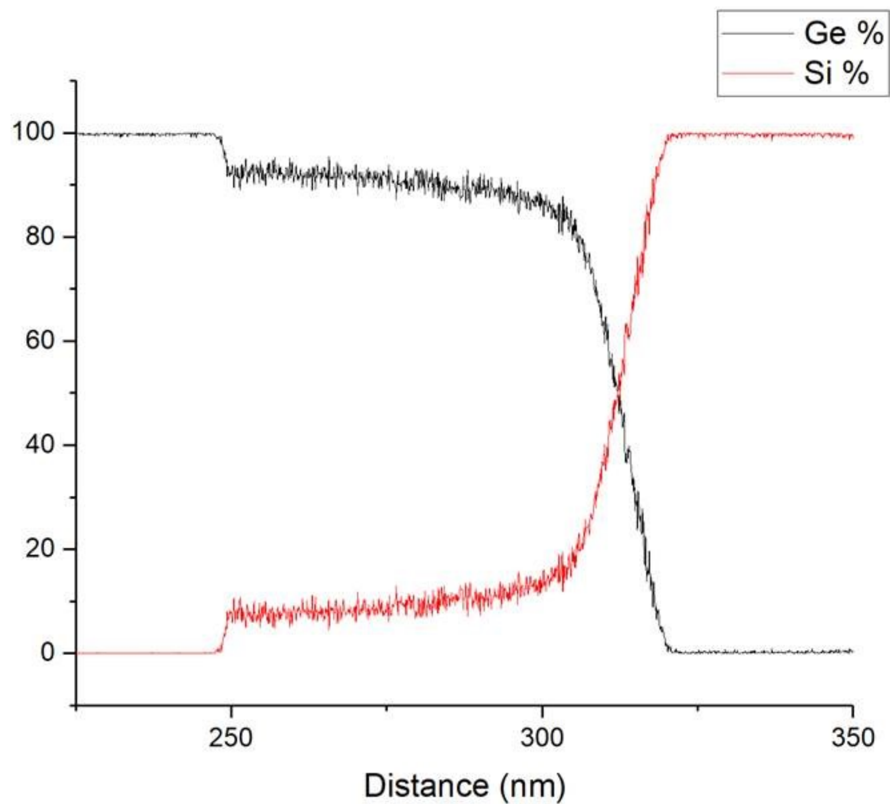

Figure S6: SIMS measurement of the Ge and Si concentration in the Si_xGe_{1-x} *layer.*

(Supporting Note 7) Row SThM data

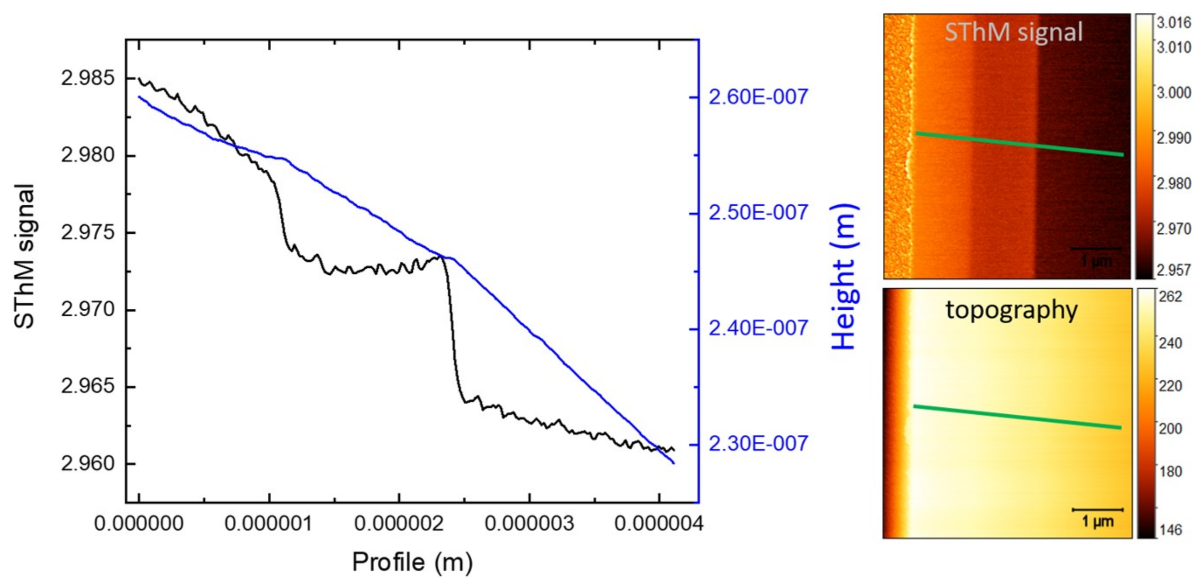

Figure S7: SThM signal and topography profiles as acquired from the row data images on the right for the sample of Si/Si_xGe_{1-x}/Ge/Ge_ySn_{1-y}. Note that the topography image is flattened. As can be seen the SThM signal within each layer is due to the thermal resistance change of the material and not due to artefacts induced by the cross sectioning.

(Supporting Note 8) SThM image of Si/SiO2 sample including the top surface

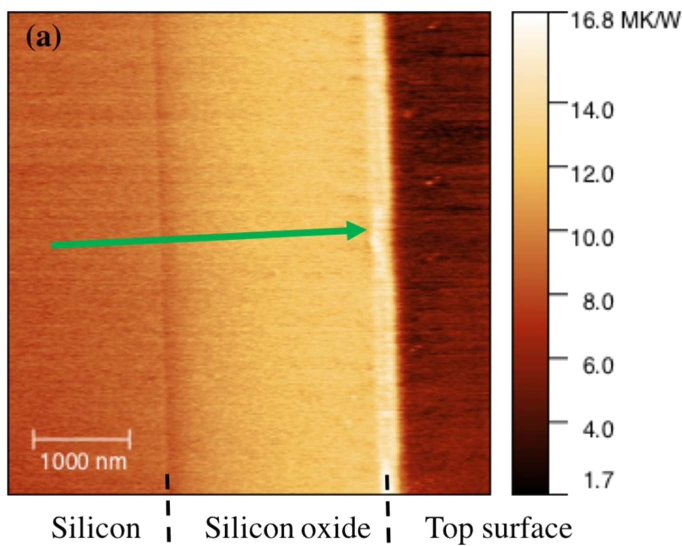

Figure S8: SThM signal of cross-sectioned Si/SiO_2 sample. The different areas of the sample are shown.

(Supporting Note 9) Zoom in figure 3 of manuscript

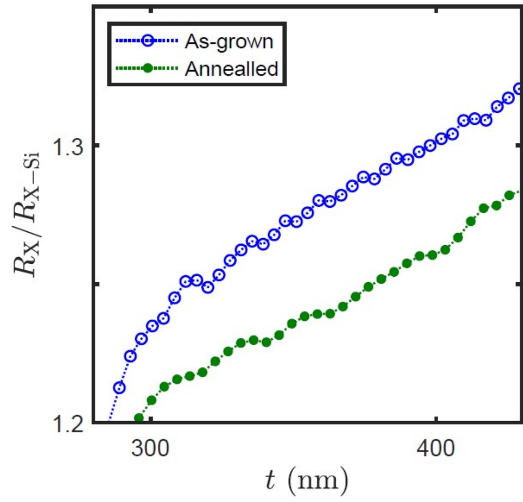

Figure S9: Thermal resistance (normalized with Si and Ge layers thermal resistance) as a function of height for as-grown and annealed samples. Zoom in the figure 3b of the manuscript.